2016

High-coercivity magnetism in nanostructures with strong easy-plane anisotropy

Balamurugan Balasubramanian
University of Nebraska–Lincoln, balamurugan@unl.edu

Priyanka Manchanda
University of Nebraska-Lincoln, priyanka.manchanda@vanderbilt.edu

Ralph A. Skomski
University of Nebraska-Lincoln, rskomski2@unl.edu

Pinaki Mukherjee
University of Nebraska-Lincoln, pinaki.mukherjee@rutgers.edu

Shah R. Valloppilly
University of Nebraska-Lincoln, svalloppilly2@unl.edu

See next page for additional authors

High-coercivity magnetism in nanostructures with strong easy-plane anisotropy

Balamurugan Balasubramanian,[1,2,a)] Priyanka Manchanda,[1,2] Ralph Skomski,[1,2] Pinaki Mukherjee,[1,2] Shah R. Valloppilly,[1] Bhaskar Das,[1,2] George C. Hadjipanayis,[3] and David J. Sellmyer[1,2,a)]

[1]*Nebraska Center for Materials and Nanoscience, University of Nebraska, Lincoln, Nebraska 68588, USA*
[2]*Department of Physics and Astronomy, University of Nebraska, Lincoln, Nebraska 68588, USA*
[3]*Department of Physics and Astronomy, University of Delaware, Newark, Delaware 19716, USA*

(Received 23 February 2016; accepted 31 March 2016; published online 15 April 2016)

We report the fabrication of a rare-earth-free permanent-magnet material Co_3Si in the form of nanoparticles and investigate its magnetic properties by experiments and density-functional theory (DFT). The DFT calculations show that bulk Co_3Si has an easy-plane anisotropy with a high $K_1 \approx -64$ Merg/cm^3 (-6.4 MJ/m^3) and magnetic polarization of 9.2 kG (0.92 T). In spite of having a negative anisotropy that generally leads to negligibly low coercivities in bulk crystals, Co_3Si nanoparticles exhibit high coercivities (17.4 kOe at 10 K and 4.3 kOe at 300 K). This result is a consequence of the unique nanostructure made possible by an effective easy-axis alignment in the cluster-deposition method and explained using micromagnetic analysis as a nanoscale phenomenon involving quantum-mechanical exchange interactions. © *2016 AIP Publishing LLC*.
[http://dx.doi.org/10.1063/1.4945987]

Finding new magnetic materials with enhanced magnetocrystalline anisotropy has been a cornerstone of scientific and technological progress in recent decades. This is of paramount importance to satisfy the increasing demand of high-anisotropy materials for a wide range of applications, such as hard-disk drives, spintronics, hybrid vehicles, wind turbines, home appliances, and biomedicine.[1–5] The highest anisotropies are now obtained in rare-earth compounds, but rare-earth price and supply uncertainties, as well as the limited range of naturally occurring compounds, call for alternative approaches. Today's permanent-magnet and magnetic-recording technologies are generally based on the set of materials whose magnetocrystalline anisotropy constants K_1 are positive. Materials with negative K_1 (easy-plane anisotropy) are typically regarded as useless for such applications, because they exhibit very low coercivities. For example, in single crystals, the coercivity H_c is often close to zero for $K_1 < 0$, because the magnetization is allowed to rotate freely.[6]

Magnetic nanoparticles can be used as building blocks to fabricate novel nanostructured materials of fundamental and technological importance.[3–5,7] Furthermore, the nonequilibrium fabrication process used for nanoclusters or particles can stabilize metastable magnetic materials and often leads to new crystal structures including those with very high magnetocrystalline anisotropies.[8,9] In this communication, we have used a non-equilibrium cluster deposition method to synthesize a rare-earth-free magnetic material Co_3Si in the form of nanoparticles and verified its crystal structure, which is a high-temperature metastable phase according to the bulk phase diagram and has not been produced previously. While density-functional theory (DFT) calculations are used to show that Co_3Si crystal has an easy-plane anisotropy, having a high $K_1 \approx -64$ Merg/cm^3, we prove using experiments and micromagnetic analysis that this negative anisotropy translates into high coercivities (17.4 kOe at 10 K and 4.3 kOe at 300 K) upon nanostructuring.

Co_3Si is an intriguing material, predicted to crystallize in the hexagonal $CdMg_3$ structure (space group P63/mmc),[10] as schematically shown in Fig. 1(a). However, the equilibrium phase diagram of Fig. 1(b) indicates that bulk Co_3Si can be stabilized only for a single composition (25 at. % Si) in a narrow temperature range of about 1190 to 1200 °C.[11,12] At lower temperatures, this phase decomposes into equilibrium phases such as εCo and Co_2Si,[12] and thus, its magnetic properties have not yet been measured. In this work, we use a non-equilibrium cluster-deposition method to produce Co_3Si nanoparticle thin films. A high direct-current power of about 200 W was used to sputter a Co-Si composite target using a mixture of argon [400 standard cubic centimeter per minute (SCCM)] and helium (50 SCCM) as sputtering gases to form Co_3Si nanoparticles in a water-cooled gas-aggregation chamber. The nanoparticles were extracted as a collimated beam before deposition on substrates kept at room temperature in the deposition chamber.

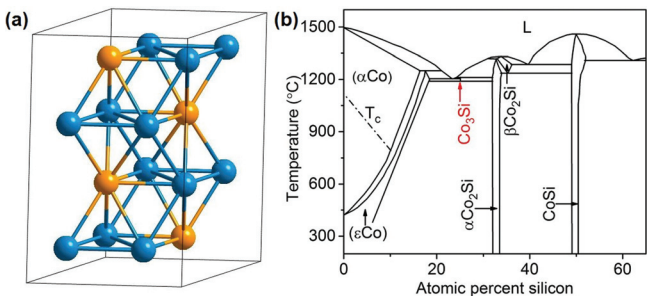

FIG. 1. Bulk Co_3Si: (a) crystal structure; (b) Co-Si phase diagram (from Refs. 11 and 12).

[a)]Electronic addresses: bbalasubramanian2@unl.edu and dsellmyer@unl.edu

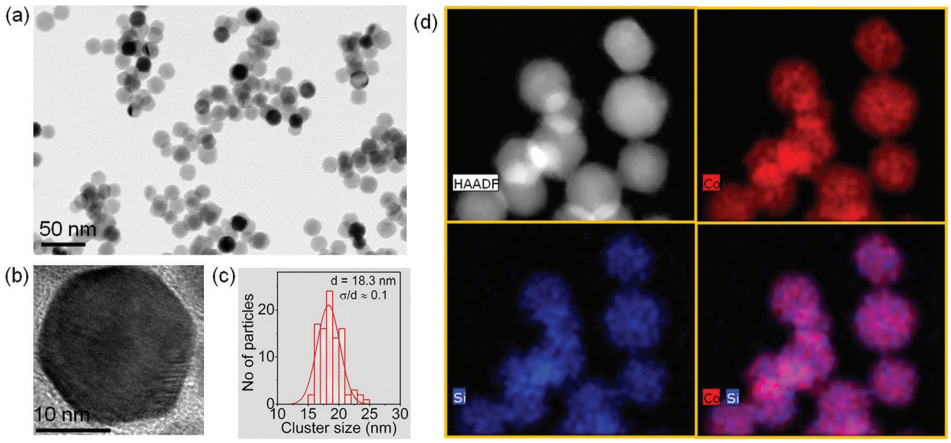

FIG. 2. TEM micrographs of Co_3Si nanoparticles: (a) A low-resolution TEM image. (b) High-resolution TEM image of a single nanoparticle. (c) The particle-size histogram revealing a narrow size-distribution. σ and d are the standard deviation and average particle size, respectively. (d) A high-angle annular dark-field image and the corresponding EDS color maps showing the color distributions of Co (red), Si (blue), and the combined Co and Si.

In order to measure more precisely the size, size-distribution, and shape, nanoparticles with low-coverage densities were deposited on carbon-coated copper grids only for transmission electron microscopy (TEM) measurements using a FEI Tecnai Osiris scanning transmission electron microscope. For x-ray diffraction (XRD) and magnetic measurements, the Co_3Si nanoparticles were deposited for extended times to form dense nanoparticle films of approximate 270 nm thickness on a single-crystalline Si (111) substrate. XRD and magnetic measurements were performed with a Rigaku D/Max-B x-ray diffractometer using a Co K_α wavelength of about 1.7889 Å and SQUID (superconducting quantum interference device) magnetometry, respectively. The growth and crystallization of nanoparticles are completed in the gas-aggregation chamber, and there is no additional growth on deposition on the room-temperature substrates. Thus, the size, shape, and structure of the Co_3Si nanoparticles do not depend on substrates and film thickness. Further, we have also used the same growth parameters to prepare the Co_3Si samples for TEM and XRD/SQUID measurements. The nanoparticle samples were capped with a thin carbon layer immediately after deposition to avoid any possible contamination such as a thin oxide formation on the surface of the nanoparticles upon exposure to air, using a radio-frequency magnetron sputtering gun employed in the deposition chamber.

To verify the hexagonal $CdMg_3$ structure, we have used TEM, scanning transmission electron microscopy (STEM), energy-dispersive x-ray spectroscopy (EDS), and XRD. The TEM images, Figs. 2(a) and 2(b), show that most nanoparticles have facets typical of hexagonal crystal structures. The particle-size histogram estimated from Fig. 2(a) shows a narrow size-distribution with a number-averaged particle size $d = 18.3$ nm and a standard deviation of $\sigma/d \approx 0.10$, as shown in Fig. 2(c).

Figure 2(d) contains a high-angle annular dark-field (HAADF) STEM image of Co-Si nanoparticles with atomic number contrast; the corresponding EDS color maps show the distribution of Co, Si, and combined Co and Si. The STEM result and a subsequent EDS analysis reveal a uniform distribution of Co and Si in the nanoparticles with a composition close to the Co_3Si stoichiometry. This result is supported by the structural analysis using high-resolution TEM (HRTEM) and XRD, Figs. 3(a)–3(e). For example, the fast Fourier transforms of the HRTEM images of two single crystalline Co-Si nanoparticles, Figs. 3(a) and 3(b), are indexed to the $CdMg_3$ along the $[1\bar{1}\bar{2}]$ and [010] zone axes in Figs. 3(c) and 3(d), respectively.

The experimental XRD patterns, Fig. 3(e), are predominantly indexed to the hexagonal Co_3Si structure, but there is also a weak and presumably (002)-textured hcp Co phase. Rietveld refinement of the XRD pattern indicates the presence of an hcp ε-Co phase of less than 10 vol. %. The experimental lattice parameters for the Co_3Si nanoparticles are $a = 4.990$ Å and $c = 4.497$ Å.

For the magnetic measurements, the nanoparticles were deposited in a magnetic field. The particles travel in the z-direction, a magnetic field is applied in the x-direction, and the deposited film plane is in the x-y-plane. A very similar field alignment method, which we have applied previously to easy-axis particles, is used to align the Co_3Si nanoparticles.[9] Figure 4 shows the experimental hysteresis loops of the

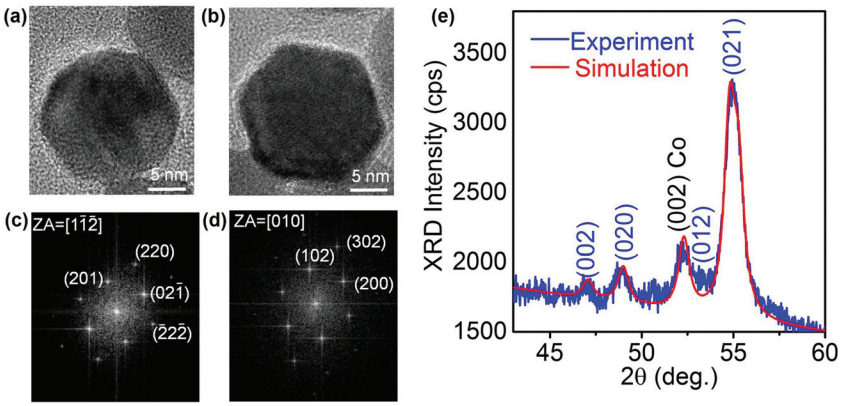

FIG. 3. Structure of Co_3Si nanoparticles: (a) and (b) high-resolution TEM (HRTEM) images. (c) and (d) Fast Fourier transforms of the HRTEM images (a) and (b), indexed to the [1 $\bar{1}$ $\bar{2}$] and [010] zone axes (ZA) of the hexagonal structure, respectively. (e) Experimental and simulated x-ray diffraction patterns.

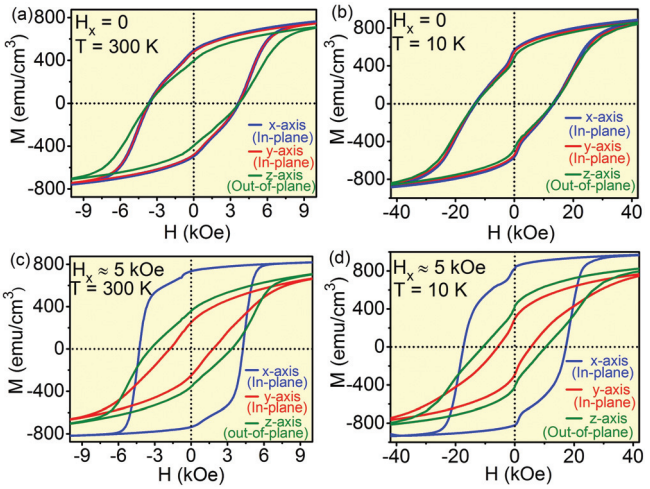

FIG. 4. Field dependence of magnetization: Hysteresis loops of nanoparticle films deposited in an alignment field, (a) and (b) $H_x = 0$ and (c) and (d) $H_x \approx 5$ kOe, where T is the measurement temperature. The measurement directions are x (blue), y (red), and z (green). The shoulders in (a)–(d) are caused by the hcp-Co minority phase and, probably, by some uncoupled easy-plane particles.

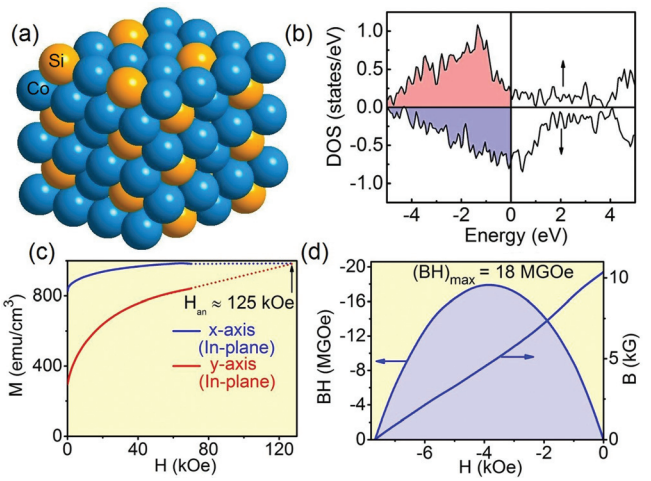

FIG. 5. Magnetization, anisotropy, and energy product: First-principle description: (a) A hexagonal Co_3Si nanoparticle containing 64 atoms and (b) total density of states. (c) The approach to saturation of magnetization in the aligned nanoparticle film at 10 K. The anisotropy field H_{an} (indicated by an arrow) is evaluated by extending the experimental easy- and hard-axis magnetization curves (dotted line) to intersect. (d) B and BH curves measured at 10 K. The maximum energy product is denoted as $(BH)_{max}$.

unaligned [(a) and (b)] and field-aligned [(c) and (d)] nanoparticle films measured at different temperatures with a SQUID magnetometer. Blue, red, and green indicate that the magnetization is measured in the x, y, and z directions, respectively. The nanoparticle films show high H_c, for example, (17.4 kOe at 10 K) and (4.3 kOe at 300 K) for the aligned film.

To understand the magnetic behavior, we have performed first-principle calculations in the framework of the DFT, using projected augmented method (PAW) as implemented in the Vienna *ab-initio* simulation package (VASP).[13] For this, we have considered both bulk and Co_3Si nanoparticle structures and used the experimental lattice parameters. The exchange-correlation effects were treated using generalized gradient approximation–Perdew-Burke-Ernzerhof (GGA-PBE),[14] and an energy cut-off of 450 eV for plane-wave expansion of the PAWs was used. For the bulk calculations, $11 \times 11 \times 11$ Monkhorst-Pack grid for k-point sampling was used,[15] and in the case of the nanoparticles, the Γ-point is used for k-point sampling. The 64-atom Co_3Si nanoparticle was placed in a cubic supercell with an edge length of 30 Å to exclude interactions between neighboring particles. The atomic positions for the nanoparticles and bulk alloy are fully relaxed until the force acting on each atom is less than 0.01 eV/Å. A convergence criterion of 10^{-6} eV was used for electronic structure.

Figure 5 shows a nanoparticle having 64 atoms (a) and the corresponding total density of states (b). The theoretical zero-temperature saturation magnetic polarization J_s for the nanoparticles 9.6 kG (1.34 μ_B/Co) is somewhat higher than the theoretical bulk magnetic polarization of 9.2 kG (1.28 μ_B/Co), where $J_s = 4\pi M_s$ (M_s = saturation magnetization). This is due to a moderately enhanced magnetization at the particle surface, which is a rather common phenomenon, caused by the reduced coordination number of the Co atoms near the surface.[16] In this study, our DFT calculations show that the surface Co atoms exhibit slightly higher moments of about 1.4–1.5 μ_B, as compared to the "core" atoms that have about 1.2–1.3 μ_B.

The calculated total-energy difference between spin orientations in the (100) and (001) directions yields a magnetocrystalline anisotropy energy of −3.9 meV per unit cell (2 formula units) for the bulk Co_3Si crystal, which corresponds to $K_1 = -64$ Merg/cm^3. The magnitude of this anisotropy is large and comparable to that of typical rare-earth easy-axis intermetallics,[17] but its sign is negative rather than positive.

At first glance, Figs. 4(c) and 4(d) look like easy-axis anisotropic behavior, $K_1 > 0$. Easy-plane single crystals have negligible coercivity, in striking contrast to the observed high coercivities, for example, 17.4 kOe at 10 K and 4.3 kOe at 300 K in the aligned nanoparticle films. To estimate the low-temperature anisotropy, we use the calculated saturation magnetic polarization of nanoparticles and extrapolate, yielding an anisotropy field H_a of about 125 kOe, corresponding to the point where the easy- and hard-axis magnetization curves intersect, as shown by the dotted lines in Fig. 5(c). The well-known relation $H_a = 2K_{eff}/M_s$ then gives an effective anisotropy constant of $K_{eff}^{exp} = 48$ Merg/cm^3 that subsequently leads to high coercivities. The high coercivities and saturation magnetizations of the aligned Co_3Si nanoparticle films translate into $(BH)_{max} = 18$ MGOe, as shown in the B and (BH) curves measured at 10 K [Fig. 4(d)], where $B = H + 4\pi M$ is the magnetic field induction or flux density. Similarly, the aligned nanoparticle film exhibits $(BH)_{max} = 12$ MGOe at 300 K (not shown here). $(BH)_{max}$ as determined from the hysteresis loop is often measured for dense-packed nanoparticles to understand their energy products, assuming they can be used as building blocks to produce bulk magnets. Although scale up of the cluster-deposition process to produce magnetic materials in bulk quantities remains a significant challenge, our approach provides useful insights and fundamental understanding for developing future nanoparticle-based permanent-magnet materials.

Figure 6 explains the difference between the theoretical prediction $K_1^{th} = -64$ Merg/cm^3 and the experimental estimate $K_{eff}^{exp} = 48$ Merg/cm^3. Easy-plane and easy-axis

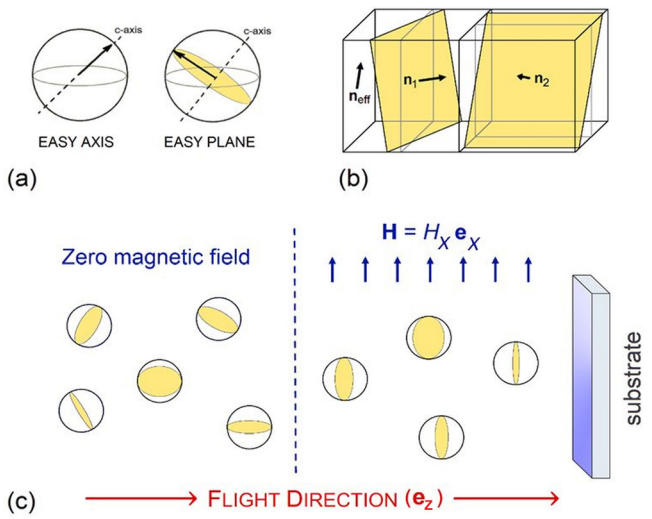

FIG. 6. Easy-plane micromagnetism: (a) difference between easy-axis and easy-plane uniaxial anisotropies. (b) Formation of an effective easy axis $n_{eff} \sim n_1 \times n_2$ due to interparticle exchange. (c) Realization of an easy axis $n_{eff} = e_x$ during cluster deposition. The arrows in (a) show preferential magnetization directions, and yellow areas correspond to easy planes.

nanoparticles show very different field-alignment (a) and exchange-coupling (b) behaviors. Field alignment of easy-axis particles completely fixes the crystallographic *c*-axis, whereas field-alignment of easy-plane particles merely ensures that the easy plane (yellow) contains the field direction (c). When field-aligned easy-plane nanoparticles arrive at the surface, the particles' *c*-axes are randomly distributed in the *x*-*y* plane, and the particles' magnetizations are free to rotate in each easy plane.

However, the packing of the nanoparticles on the film is dense, which causes the particles to undergo a ferromagnetic exchange coupling with a spatial range of the order of 10 nm. Due to this exchange, the particles minimize their total energy by magnetization rotation in their easy planes. Inspection of Fig. 6(c) shows that the only magnetization direction that simultaneously minimizes the anisotropy energies of all neighboring nanoparticles is the *x*-direction—all yellow planes in (c) contain the *x*-axis. The exchange interaction therefore creates an effective easy axis. To evaluate the strength of the resulting net anisotropy, it is necessary to average over all *c*-axis nanoparticle orientations in the *x*-*y* plane. The result is $K_{eff}^{th} = \frac{|K_1^{th}|}{2}$ corresponding to $K_{eff}^{th} = 32$ Merg/cm^3. The experimental K_{eff}^{exp} of the nanoparticles (48 Merg/cm^3) is higher than the theoretical bulk value, but they are similar and in reasonable agreement.

In conclusion, we have synthesized a rare-earth-free magnetic material Co_3Si in the form of nanoparticles with high coercivities, high saturation polarization, and appreciable energy products. First-principle calculations show that Co_3Si possesses a very high but negative easy-plane anisotropy. Micromagnetic analysis explains how easy-plane anisotropy leads to easy axis behavior at the nanoscale via exchange coupling and subsequently yields high experimental coercivities for Co_3Si nanoparticles. This work establishes a class of high-anisotropy magnetic materials, not containing rare earths or other expensive metals and shows a path towards fabrication of nanoparticle-based bulk magnetic materials with easy-plane anisotropies, useful energy products, and containing earth-abundant elements.

Synthesis, experimental characterization, and theoretical analysis were primarily supported by the U.S. Department of Energy, Office of Basic Energy Sciences under the Award No. DE-FG02-04ER46152 (B.B., R.S., S.R.V., B.D., and D.J.S.) and DE-FG02-04ER4612 (G.C.H.). Electron microscopy analysis and electronic structure calculations were supported by the U.S. Army Research Office under the Award No. WF911NF-10-2-0099 (P.M. and P.M.). Research at Nebraska was performed in part in the Nebraska Nanoscale Facility, Nebraska Center for Materials and Nanoscience, which is supported by the National Science Foundation under Award NNCI: 1542182, and the Nebraska Research Initiative. This research also benefited from the Holland Computing Center (simulations).

[1]D. Kramer, Phys. Today **63**(5), 22 (2010).
[2]N. Jones, Nature **472**, 22 (2011).
[3]D. J. Sellmyer, Nature **420**, 374 (2002).
[4]J. Kim, S. E. Chung, S.-E. Choi, H. Lee, J. Kim, and S. Kwon, Nat. Mater. **10**, 747 (2011).
[5]J.-H. Lee, J.-T. Jang, J.-S. Choi, S. H. Moon, S.-H. Noh, J.-W. Kim, J.-G. Kim, II-S. Kim, K. I. Park, and J. Cheon, Nat. Nanotechnol. **6**, 418 (2011).
[6]J. M. D. Coey, *Magnetism and Magnetic Materials* (The University Press, Cambridge, 2009).
[7]J. Jellinek, Faraday Discuss. **138**, 11 (2008).
[8]A. N. Baranov, P. S. Sokolov, V. A. Tafeenko, C. Lathe, Y. V. Zubavichus, A. A. Veligzhanin, M. V. Chukichev, and V. L. Solozhenko, Chem. Mater. **25**, 1775 (2013).
[9]B. Balamurugan, B. Das, V. R. Shah, R. Skomski, X. Z. Li, and D. J. Sellmyer, Appl. Phys. Lett. **101**, 122407 (2012).
[10]ICDD, International Centre for Diffraction Data, Card No. 04-001-3215, 2014.
[11]H. Okamoto, *Phase Diagram of Binary Alloys* (ASM, Materials Park, 2000), p. 259.
[12]K. Ishida, T. Nishizawa, and M. E. Schlesinger, J. Phase Equilib. **12**, 578 (1991).
[13]G. Kresse and D. Joubert, Phys. Rev. B **59**, 1758 (1999).
[14]J. P. Perdew, K. Burke, and M. Ernzerhof, Phys. Rev. Lett. **77**, 3865 (1996).
[15]H. J. Monkhorst and J. D. Pack, Phys. Rev. B **13**, 5188 (1976).
[16]B. Balasubramanian, P. Manchanda, R. Skomski, P. Mukherjee, B. Das, T. George, G. C. Hadjipanayis, and D. J. Sellmyer, Appl. Phys. Lett. **106**, 242401 (2015).
[17]R. Skomski, J. Phys.: Condens. Matter **15**, R841 (2003).